

TRACING INTERSTELLAR MAGNETIC FIELD USING THE VELOCITY GRADIENT TECHNIQUE (II)

KA HO YUEN^{1,2}, A. LAZARIAN¹

¹Department of Astronomy, University of Wisconsin, Madison

²Department of Physics, The Chinese University of Hong Kong

ABSTRACT

This study proceeds with the development of the technique employing velocity gradients that were identified in [González-Casanova & Lazarian \(2016\)](#) as a means of probing magnetized interstellar media. We demonstrate a few practical ways of improving the accuracy of tracing magnetic fields in diffuse interstellar media using velocity gradients. We show that the higher order velocity centroids are able to provide better tracing of magnetic fields compared with the first order velocity centroids that have been used so far. Another way of improving the tracing that we explore is based on removing from the analysis the regions of strong shocks, which we identify using both by the increase of the amplitude of the velocity and density gradients and the misalignment of the two gradient measures. Addressing the magnetic field tracing in superAlfvénic turbulence we introduce the procedure of filtering of low spatial frequencies that enables magnetic field tracing in the situations when the kinetic energy of turbulent plasmas dominate its magnetic energy. We provide theoretical and numerical arguments as to why we expect that the velocity gradients trace magnetic fields in diffuse media better than density gradients. We also demonstrate this by comparing the alignment of the velocity centroid gradients (VCGs) as well as intensity gradients (IGs) obtained with the GALFA HI survey and the Planck polarization data that traces magnetic field in the cold and warm diffuse atomic hydrogen. Finally, by using the simulations with self-gravity we demonstrate that in the regions of the gravitational collapse the alignment of the VCGs changes with respect to the magnetic field.

Keywords: ISM: general — ISM: structure — magnetohydrodynamics (MHD) — radio lines: ISM — turbulence

1. INTRODUCTION

Interstellar media are turbulent with magnetic fields playing a critical role in the key processes, including star formation, propagation and acceleration of cosmic rays as well as regulating heat and mass transfer between different phases. Therefore it is essential to have a reliable way of studying magnetic fields. Unfortunately, there only a few ways of tracing magnetic fields and their applicability is limited. For instance, tracing magnetic fields with aligned grains (see [Lazarian 2007](#)) requires either the availability of the background stars, if the polarization via extinction is employed, or sensitive far infrared measurements, which frequently imply the use of the space-based instruments. Another major technique that employs synchrotron polarization mostly traces magnetic fields in the hot phase of the ISM (see [Draine 2011](#)).

Using spectroscopic data for tracing magnetic fields was suggested and demonstrated in [Lazarian et al. \(2002\)](#) using the anisotropy of correlation functions of the velocity channel maps. The new approach was motivated by the theoretical advancements establishing that the MHD turbulence is anisotropic ([Goldreich & Sridhar 1995](#), hereafter GS95. See also [Lazarian & Vishniac 1999](#); [Cho & Vishniac 2000](#);

[Maron & Goldreich 2000](#); [Kowal & Lazarian 2010](#), see [Brandenburg & Lazarian 2013](#) for a review) and should translate into the anisotropy of the observed fluctuations. Later the technique was extended with the use of velocity centroids [Esquivel & Lazarian \(2005\)](#) and [Brunt & Heyer \(2002\)](#) using the Principal Component Analysis (PCA) of the spectroscopic data. In its PCA incarnation the idea of tracing magnetic field anisotropies was applied to the observational data in [Heyer et al. \(2008\)](#) with the results of anisotropies shown to be consistent with the starlight polarization measurements. Further development of the technique resulted in the development of techniques using the anisotropies for obtaining the media magnetization, as it parameterized by the Alfvén Mach number ([Esquivel & Lazarian 2005](#); [Esquivel et al. 2015](#); [Tofflemire et al. 2011](#)) and the separation of compressible and incompressible turbulence components of observational data as discussed in [Kandel et al. \(2016, 2017\)](#)

A new technique for turbulence study that traces magnetic fields with velocity fluctuations was introduced in [González-Casanova & Lazarian \(2016, henceforth GL16\)](#). Instead of appealing to anisotropic velocity fluctuations as in the aforementioned approach, the new technique made use of velocity gradients that, according to the MHD turbulence theory, are maximally perpendicular to the local direction of the magnetic field. This idea was further developed in [Yuen & Lazarian \(2017, henceforth YL17\)](#) where a robust procedure for velocity centroid gradient calculations was suggested. In the

latter paper we also applied the new technique to the GALFA 21 cm data and demonstrated a good correspondence between the magnetic field tracing using Velocity Centroid Gradients (VCGs) and the magnetic field tracing with Planck polarization arising from aligned grains. This result motivates the numerical study of VCGs properties that we undertake in this paper.

As a separate development we refer to the studies of densities in relation to magnetic field tracing. In particular, [Soler et al. \(2013\)](#) reported the alignment of density gradients and magnetic fields and [Clark et al. \(2015\)](#) demonstrated that the density filaments observed by GALFA are well aligned with magnetic fields as measured by Planck polarization. In view of our previous discussion, this is a complementary development. MHD turbulence can imprint some of its properties to density, making its statistics at low sonic Mach numbers anisotropic (see [Cho & Lazarian 2003](#); [Beresnyak et al. 2005](#); [Kowal et al. 2007](#)). While both from theory and simulations we expect the density to be a worse tracer of magnetic fields, the very differences between the velocity and anisotropies can be informative of the properties of the turbulent media. For instance, the differences are expected to increase with the sonic Mach number. Our previous studies in GL16 and YL17 have, indeed, demonstrated the advantages of the VCGs compared to the Intensity Gradients (IGs) that reflect the density statistics. In this paper we further explore the differences in magnetic field tracing by the VCGs and the IGs, but search for more synergy between the two.

In addition, we want to mention that the properties of velocities and magnetic field in MHD turbulence cascade¹ (see [Lithwick & Goldreich 2001](#); [Cho & Lazarian 2002, 2003](#); [Kowal et al. 2009](#)) are rather similar and therefore one can expect the magnetic field gradients to be well aligned with velocity gradients. The new technique employing the Synchrotron Intensity Gradients (SIGs) was introduced in [Lazarian et al. \(2017\)](#), henceforth LYLC). The SIGs can trace magnetic fields in the hot and warm diffuse synchrotron emitting gas and therefore is complementary to VCGs that trace magnetic fields in the Cold and Warm phases of the ISM.

Self-gravity is expected to modify the properties of the flow in the vicinity centers of the gravitational collapse. The change of the properties of MHD turbulence within such regions is expected to be the result of VCGs changing their properties, in particular their alignment with the magnetic fields. The density distribution is even more affected by self-gravity. Indeed, a recent study by [Soler et al. \(2013\)](#), reported that the IGs rotate with respect to magnetic fields in super-Alfvénic high density self-gravitating regions. We address the issue of how VCGs and IGs behave in the regions of self-dominant gravity for the case of sub-Alfvénic clouds.

In what follows we briefly explain our numerical approach

¹ The decomposition into MHD modes suggested and performed first in [Cho & Lazarian \(2002, 2003\)](#) and later, using a different technique in [Kowal et al. \(2009\)](#) shows that the MHD turbulence cascade can be presented as three cascades with little energy exchange between them. This statement corrected the earlier assertions in the literature that the fast decay of MHD turbulence was attributed to the strong coupling of the compressible and Alfvénic modes of MHD turbulence.

in §2. We provide a comparison of the alignment of VCGs and IGs with magnetic fields in §3. We explore the properties of the VCGs in a sub-Alfvénic self-gravitating cloud in §4 and explore their synergetic use with the IGs. We discuss the underlying physics of gradients in §5. We compare our methods to recently available method in §6. We summarize our results in §7.

2. METHOD

As there are many factors affecting the alignment of rotated gradients with magnetic fields, we investigate VCGs and IGs through studying MHD simulations in different physical conditions. Following YL17 and LYLC, we used a series of compressible, turbulent, isothermal single fluid magnetohydrodynamic (MHD) simulations for examination of VCGs and IGs from ZEUS-MP/3D ([Hayes et al. 2006](#)), a variant of the code ZEUS-MP ([Norman 2000](#)). We set up simulation cubes with several combinations of sonic Mach number M_s and Alfvénic Mach number M_A , which are listed in table 1. For supersonic simulations, we increase the resolution of the simulations to ensure the cube has a sufficiently long inertial range for high M_s cases. The initial magnetic field is along the z-axis. We injected turbulence using the same method in YL17.

Table 1. Simulations used in our current work. The magnetic criticality Φ is set to be 2 for all simulation data.

Model	M_s	M_A	Resolution
b31	0.4	0.4	480 ³
b41	0.132	0.4	480 ³
b51	0.04	0.4	480 ³
c1	5	0.2	792 ³
c2	5	0.4	792 ³
c3	5	0.6	792 ³
c4	5	0.8	792 ³
c5	5	1.0	792 ³
c6	5	1.2	792 ³
c7	5	1.4	792 ³
c8	5	1.6	792 ³
c9	5	1.8	792 ³
c10	5	2.0	792 ³
d	5	0.2	360 ³

The projection maps and the respective gradients were computed following the recipe of YL17. Assuming the line-of-sight direction x , the intensity $I(\mathbf{r})$, velocity centroid $C(\mathbf{r})$ are defined as

$$\begin{aligned}
 I(\mathbf{r}) &= \int \rho(\mathbf{r}, x) dx \\
 C(\mathbf{r}) &= I^{-1} \int \rho(\mathbf{r}, x) v_x(\mathbf{r}, x) dx
 \end{aligned}
 \tag{1}$$

We also computed polarization by assuming the emissivity is a constant over the line of sight. In other words, the Stokes parameter $Q(\mathbf{r}), U(\mathbf{r})$ can be expressed in terms of $\theta = \tan^{-1}(B_y/B_z)$, where $B_{y,z}$ are the y and z direction

magnetic fields:

$$\begin{aligned} Q(\mathbf{r}) &= \int \cos(2\theta(\mathbf{r}, x)) dx \\ U(\mathbf{r}) &= \int \sin(2\theta(\mathbf{r}, x)) dx \end{aligned} \quad (2)$$

The polarized intensity $P = \sqrt{Q^2 + U^2}$ and angle $\phi = 0.5 \tan^{-1}(U/Q)$ are then defined correspondingly.

Most of our paper is devoted to the studies of diffuse media with the negligible effects of gravity. In section §4 we briefly deal with the case of strongly magnetized media for which self-gravity is important. To simulate this setting we turn on gravity after turbulence is saturated. To trace the effect of gravity with respect to time, we take several snapshots with even time intervals before and after the presence of gravity. We stop our calculation when any pixel in the system violates the Truelove criterion (Truelove et al. 1997), which tells when to stop the simulation before having numerical artifacts due to self-gravitating collapse. To examine how the relative strength of gravity within magnetic fields affects the system, we examine cubes with same sonic and Alfvénic Mach number but different gravity to magnetic field ratios.

3. ALIGNMENTS BETWEEN VCG/IG AND MAGNETIC FIELD

To compare the performance between VCGs and IGs, we employed the *alignment measure*

$$AM = 2\langle \cos^2 \theta_r \rangle - 1, \quad (3)$$

(see GL16, YL17), to measure the relative alignment between *rotated* gradients and magnetic fields. A perfect alignment gives $AM = 1$. We examine the performance of the VCGs and IGs in various physical conditions.

3.1. How does sonic Mach number M_s affect gradient alignment?

Sonic Mach number, M_s , is the ratio of the turbulent injection velocity and the speed of sound and it reflects compressibility of the turbulent flow. High sonic Mach number is associated with the presence of shocks due to strong compression. We start with nearly incompressible simulations with $M_A = 0.4$ and $M_s = 0.04, 0.132, 0.4$ to perform an alignment test on both the VCGs and the IGs. Figure 1 shows how the VCGs and the IGs behave in subsonic systems. The alignment of the VCGs in sub-sonic systems are generally better compared with the IGs.

Supersonic turbulence will create strong density compression associated with shocks. In contrast, the approach underlying magnetic field tracing by velocity gradient is justified for the incompressible Alfvénic modes (GS95, Cho & Lazarian 2003), for which the eddies are elongated along the local magnetic field direction, causing the velocity gradients to be maximally perpendicular to the local magnetic field direction.

We also note that the VCGs trace magnetic fields better in supersonic turbulence. The reason is that density structures are indirect tracers of magnetic fields (Beresnyak et al. 2005), but they are directly influenced by shocks. To improve the

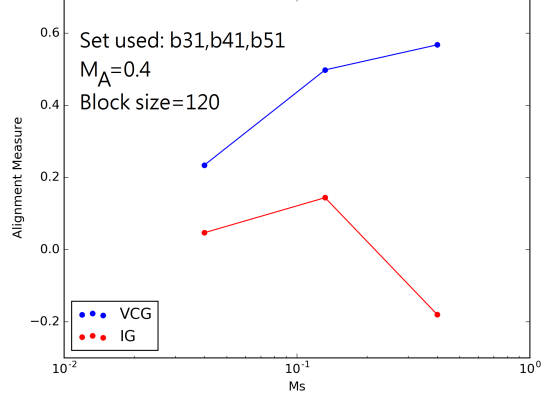


Figure 1. A diagram showing how sonic mach number affects alignment globally.

alignment in shock environments, we apply a shock isolation algorithm to our synthetic maps. To start with we focus on removing the shock with jumps (J-shocks). For Jump discontinuity, the change of density across the shock is very significant compared to the surrounding environment. Therefore a higher density gradient amplitude is found across the shock front. Hence we sort out the gradient data according to their gradient amplitude, and check the alignment on the slice of gradient data using a $M_s = 5$ map in Figure 2 for both the VCGs and the IGs. Given the gradient amplitude x , and the global mean μ , the standard deviation σ , the Z-score of x is defined as $Z(x) = (x - \mu)/\sigma$. A higher positive Z-score stands for regions with gradient amplitude above the system average. Regions with higher amplitude correspond to those with J-shocks. We only plot regions with positive Z-scores. Figure 2 shows that higher gradient amplitude tend to have weaker alignment. For simplicity, we compute the alignment without applying the sub-block average. That means that the data points in 2 are being classified only by their respective gradient amplitudes. Different phases of the ISM are expected to have different sonic Mach numbers M_s . The Mach number M_s of warm gas is of the order of unity (see Gaensler et al. 2011 and ref. therein), while the Mach number of cold interstellar media (see Draine 2009) as well as molecular clouds can be 10 and even higher. This makes the procedures of removing pixels affected by shocks relevant. We may expect that removing pixels with higher gradient amplitudes could help improving the performance of gradient technique. At the same time, the pixels that we remove for the gradients to work better carry the information about the shocks and such regions can be studied separately.

We do, however, have to emphasize that that this is only a preliminary study of the effects of the shocks and their removal. A more detailed analysis will be presented elsewhere.

3.2. How does Alfvénic Mach number M_A affect gradient alignment?

Aside from M_s , the Alfvénic Mach number M_A is another characteristic of the properties of turbulence. It expresses the ratio of the turbulent velocity to the Alfvén velocity. Therefore for large M_A turbulent motions are not af-

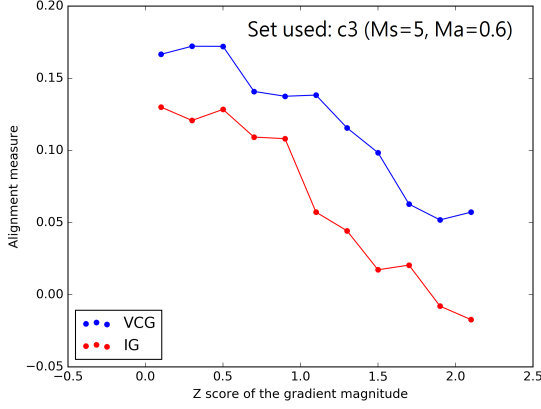


Figure 2. A scatter plot showing how VCG AM depends on the intensity gradient amplitude.

ected by magnetic fields. The turbulent cascade is different when M_A is less than 1 or larger than 1 (See Lazarian & Vishniac 1999; Esquivel & Lazarian 2005). When $M_A < 1$, $k_{\parallel} \propto k_{\perp}^{2/3}$ (Goldreich & Sridhar 1995). On the other hand, for $M_A > 1$ the nature of the cascade changes at a particular scale $l_A = LM_A^{-3}$, where L is the injection scale (Lazarian 2006). When $1/l_A < 1/k < L$, the motions are of a hydrodynamic nature, while for smaller scales the GS95 cascading takes over. Therefore we may expect that our reasoning based on GS95 theory may not work for this range of spacial scales.

We test the alignment for systems with various M_A . In this test, we use the whole set C in Table 1. Figure 3 shows the morphology of VCGs (rotated 90 degrees) as well as the projected magnetic field. For trans-Alfvénic systems in the lower panels, the rotated velocity gradient vectors trace magnetic fields reasonably well, which is consistent with our earlier results in YL17 and González-Casanova & Lazarian (2016). On the other hand, as expected, gradients in super-Alfvénic turbulence behave differently. The motion scales larger than l_A are hydrodynamic (see Lazarian 2006) and thus the alignment of gradients at these scales is different from that related to sub-Alfvénic motions. To mitigate the effect of super-Alfvénic motions, we introduce a low wavenumber filtering: we remove Fourier modes with the wavenumber below a certain threshold. We know from LYLC that removing low spatial frequencies does not much affect the tracing of magnetic fields by gradients and therefore we can expect that magnetic fields can be traced by the VCGs in the super-Alfvénic turbulence.

We computed the VCG map obtained after filtering low spatial frequencies in the direction of the projected magnetic field. Figure 4 shows the result of the alignment when wavenumbers corresponding to the scales larger than, respectively, 10, 20, 30, 40 and 50 pixels are being removed from a selected cube with resolution 792^3 . We observe that as we remove the contribution from lower wavenumbers, the alignment between the VCGs and projected magnetic fields is gradually increasing. This result matches with our theoretical expectations, as we remove the contribution of the hydrodynamic-type cascade (see Lazarian 2006).

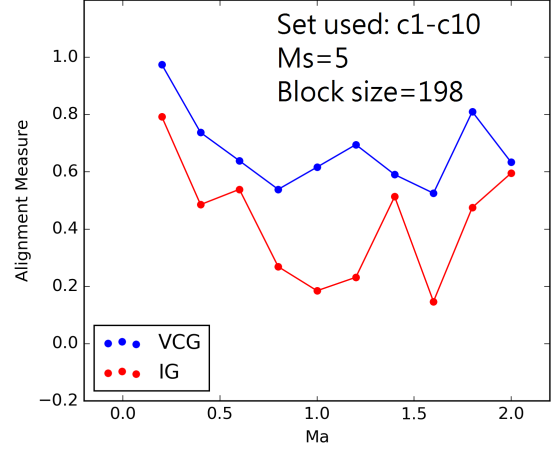


Figure 3. A scatter plot showing the alignment of VCGs and IGs in different M_A .

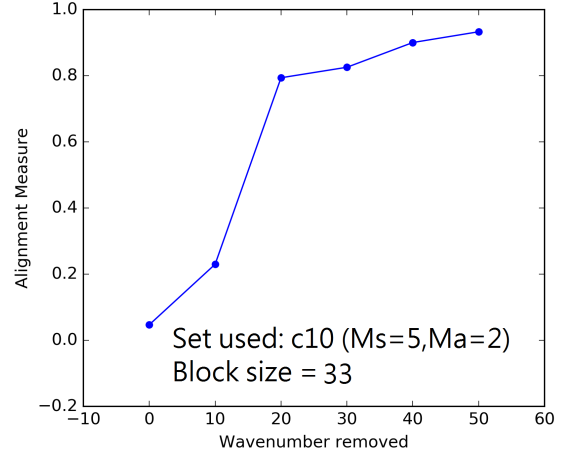


Figure 4. A scatter plot showing how the wavemode removal algorithm works.

Since the anisotropy exists for large scales in sub-Alfvénic systems, the removal algorithm does not change the alignment when facing strong field cases. We should also emphasize that, such calculations are also being performed in the synchrotron intensity gradients (SIG) in LYLC. The same conclusion from our previous work and here suggests users of the gradient technique are advised to remove the small wavenumber contributions, i.e. produce the low- k filtering of their data before applying the gradient technique. Elsewhere we will explore the optimization of filtering procedures.

3.3. How does line of sight in the B -direction affect gradient alignment?

In the general case it is natural to assume that the mean magnetic field has two components perpendicular to the line of sight and a non-zero component parallel to the line of sight. As we discussed earlier, in strong field scenarios, fluid motions are different along and perpendicular to the magnetic field, i.e. the eddies are elongated along the magnetic field.

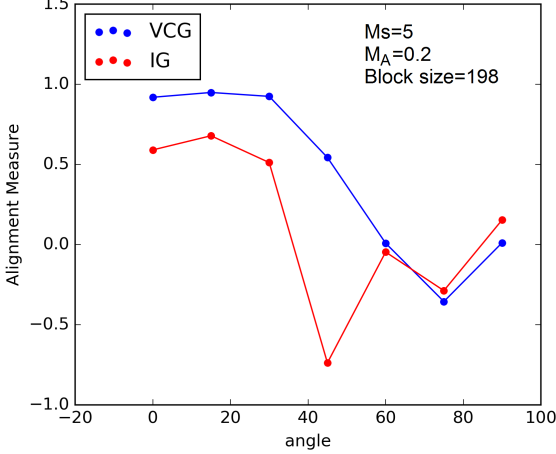


Figure 5. The AM of VCGs (Blue) and IGs (Red) with respect to the angle of rotation. Defining the line of sight when it is perpendicular to magnetic field to be 0° rotation, and parallel as 90° , we compute AM in the projected map.

The motions look different when viewed from an oblique angle. To study this effect we perform calculations of gradients changing the angle between the line of sight and the mean magnetic field.

We introduced a rotation-projection algorithm (RPA) to mimic the projected maps when the cube is being viewed from different directions. The idea of RPA is to get the rotated coordinates of the rotated three-dimensional cube through oblique projection on a predefined discrete rectangular coordinate plane. For each pixel on the projected plane, it accumulates the data from the three dimensional data with the same integral plane-of-sky coordinates, this mimics the line-of-sight observation. As the number of samples accumulated in the projected plane pixels are different, we perform a simple weighting of the contributions along the line according to the number of samples. Notice that the periodicity of the simulation domain enables us to perform such an action without worrying about the boundary conditions. To smooth the effect from grids, we apply a Gaussian prefilter of $\sigma = 2$ pixels, similar to the noisy environment in treatments of noises in LYLC. Figure 5 shows the change of AM with respect to the projection angle. We observe that the AM of the IGs is highly affected by the line-of-sight effect. At the same time, the alignment of the VCGs has a more regular behavior, with the AM gradually decreasing as the angle of rotation approaches 90° .

4. VCGS IN SELF-GRAVITATING REGIONS

All of the above was does applied to the diffuse gas where MHD turbulence is not modified by self-gravity effects. In molecular clouds we expect that the effects of self-gravity are going to be important. We expect that both velocity and density statistics respond to self-gravity but their response can be different. Below we provide the first study of self-gravity on the VCGs and this study is limited by the case of dynamically important magnetic fields.

4.1. Theoretical considerations

Self-gravity changes the motion of magnetized turbulent fluid. An additional acceleration induced by gravity is expected to modify the GS95-type anisotropy. The relative importance of gravity to magnetic field, which is measured by the magnetic criticality $\Phi \propto \sqrt{F_{grav}/F_{mag}}$, determines the properties of the turbulence. As a result, velocity gradients carry information about systems with different Φ . Below we explain the change of the VCGs induced by gravity. In parallel, we discuss what is expected from the IGs.

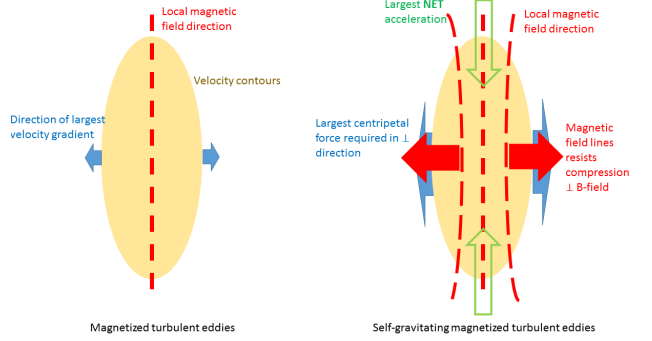


Figure 6. Illustrations on how self-gravity changes the maximum gradient direction. When gravity is absent (Left), eddies are elongated parallel to the local magnetic field direction. Assuming that the gravity center is at the center of the contours we expect a change in the velocity field (Right).

We assume the gravitational center is located at the center of an eddy in Figure 6. The velocity contour, which is equivalent to the streamlines of 90° rotated velocity gradients, is the densest perpendicular to the local magnetic field direction. Inward acceleration is governed by the density distribution of matter. For the dynamically important magnetic field we expect that in the direction perpendicular to the magnetic field, the gravitational pull inducing the acceleration is counteracted by a magnetic force. Hence, the gravitational pull induces the largest acceleration of plasma in the direction parallel to the magnetic field. This acceleration causes the gradients of velocities to turn parallel to the magnetic field.

In terms of the VCGs near the gravity center, the direction of velocity gradients gets *parallel* to magnetic field instead of being *perpendicular* to magnetic field. On the other hand, the rotation for the IGs depends on the shape of the self-gravitating core during collapse. If the flat structure perpendicular to the magnetic field is formed, we expect the IGs to also be parallel to the magnetic field. At the same time, in regions away from the gravitational center, the velocity gradient should still be perpendicular to local magnetic field, similar to the case of diffuse media that we studied earlier. These two effects are shown in the left and right panels of Figure 7.

In the language of the alignment measure AM, since the gradients near the gravitational center are turned by 90° , the AM of the block covering the core should gradually drop below zero. We tested this conclusion numerically and our results are shown our in Figure 9. At $t = 10$ a significant core collapse occurs, which makes the AM negative. This indicates most of the gradient vectors (both the VCGs and the

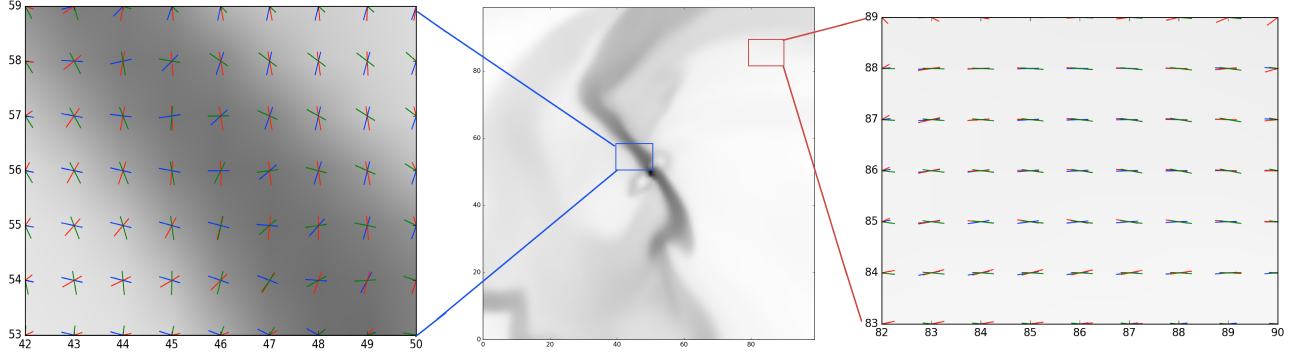


Figure 7. The morphology of the 90° rotated VCGs (Red), 90° rotated the IGs (Green) and magnetic field (Blue) on a density map, with a gravitating core in the center of the map. We select a 40×40 pixels snapshot for this core. The subpanels illustrate that the gradients behave differently at different distance from the core.

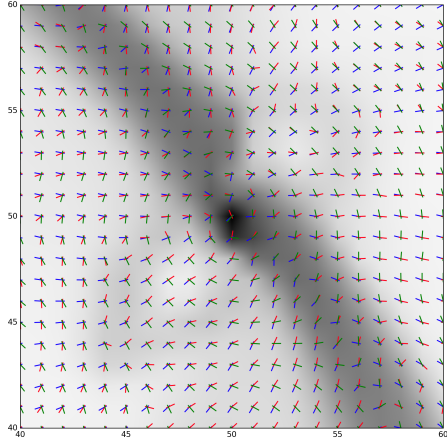


Figure 8. Similar to Figure 7, but a 20×20 pixels snapshot for this core. The density gradients are almost always perpendicular to the magnetic field. The VCGs and IGs are rotated as in YL17, just presuming themselves tracing magnetic field in diffuse regions. Both rotated VCGs (Red) and IGs (Green) show significant deviations from the magnetic field direction (Blue).

IGs) around the region tend to *align parallel* to the magnetic field direction. This is also illustrated in 8. This effect of realignment of the VCGs near the core region, together with a significant drop of AM, can signify that self-gravity is important in the given region. We believe that this is an important way of identifying the self-gravitating regions *through observational studies*.

4.2. Observational evidence

We illustrate this effect also by the data from the Galactic Arcicbo L-Band Feed Array HI Survey (GALFA-HI). We illustrate the magnetic field tracing with the VCGs and compare it to the *Planck* polarization data. In diffuse media, polarization is parallel to the local magnetic field direction see (Lazarian 2007; Andersson et al. 2015). Our chosen region from GALFA-HI survey data spans in right ascension from 15° to 60° and in declination from 4° to 16° , which is around the position of the South Pole. The bin size for the velocity

is 0.18 km/s . We also plotted the 353GHz polarization data obtained by the *Planck* satellite’s High Frequency Instrument (HFI).²

The VCGs corresponding to the right hand side ($RA \leq 35^\circ$) of Figure 10 have been already compared to the magnetic field directions given by polarization in YL17. Here, we also show the IGs. It is evident that the IGs are worse tracers of magnetic field direction compared to the VCGs. However, the misalignment of the VCGs and the IGs is informative. On the basis of our numerical experiments we can argue that the points where the VCGs and the IGs are not aligned correspond to shocks in the media.

We also see a noticeable change of alignment at the left hand side of Figure 10. There the density is increased and one may expect that self-gravity will become more important. We observe that the VCGs get less aligned with the magnetic field when the column density goes up. The misalignment is even

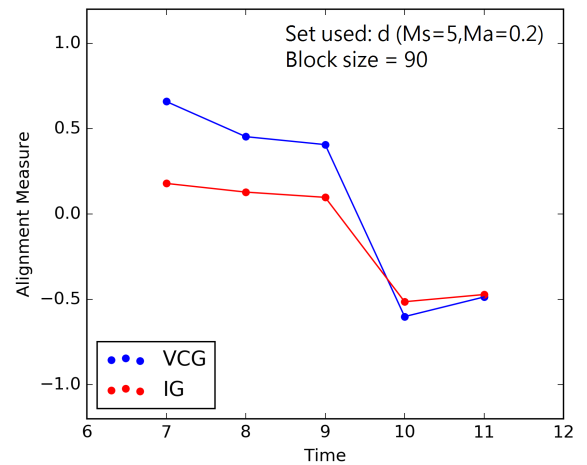


Figure 9. Response of AM for VCG and IG when gravity is introduced at $t = 7$.

² We use the *planckpy* module to extract polarization data in a particular region with J2000 equatorial coordinate: (<https://bitbucket.org/ezbc/planckpy/src>).

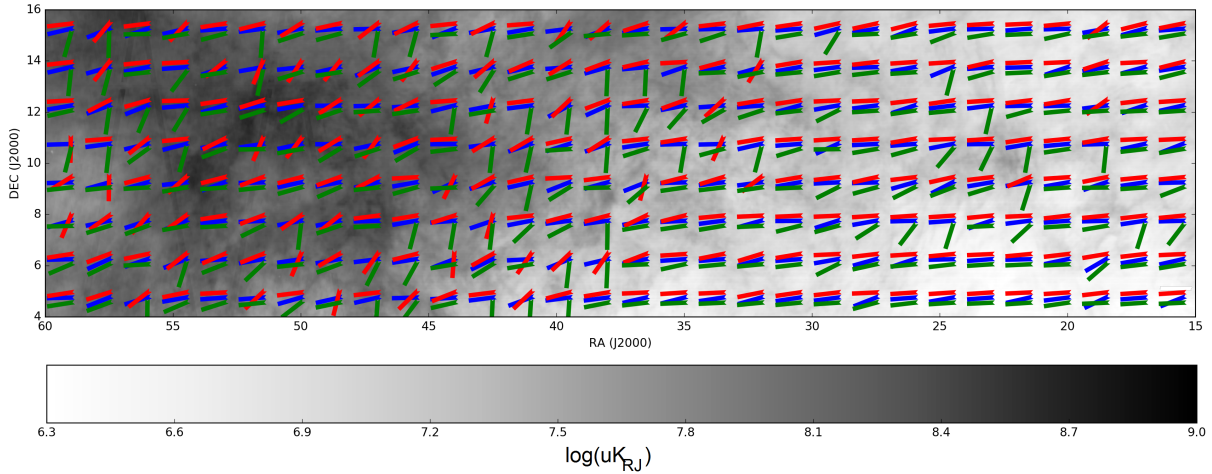


Figure 10. Gradients obtained using GALFA HI survey compared with the Planck polarization data. Here the magnetic field inferred from Planck polarization is shown using blue, while the red and green "vectors" correspond to *rotated* the VCGs and the IGs, respectively.

stronger for the IGs. We feel that this can, indeed, be interpreted as the effect of self-gravity. We intend to provide more quantitative numerical modeling of the setting elsewhere.

5. COMPARISON OF VCGS TO MEASURING ANISOTROPY OF CORRELATIONS

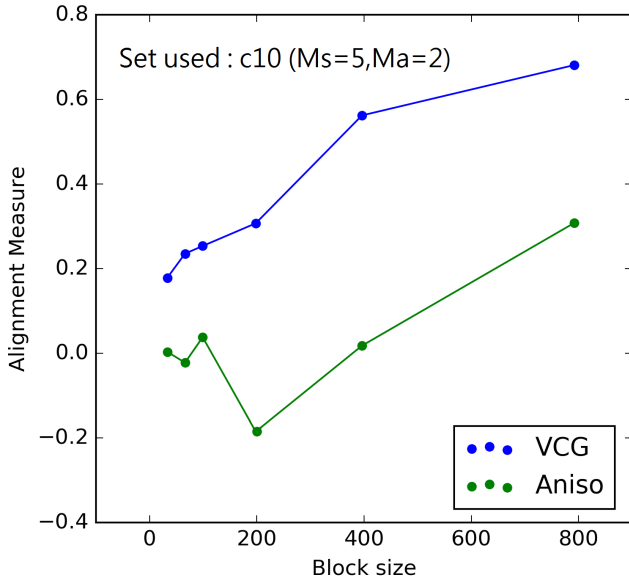


Figure 11. AM of VCG compared to that of CFA. The correlation function anisotropy of velocity centroid and intensity is calculated within the block respectively.

The anisotropic nature of MHD turbulence induces the anisotropy of observed velocity correlations. This was first demonstrated in Lazarian et al. (2002) where the velocity correlations within a channel map obtained with synthetic observations based on the result of 3D MHD turbulence were shown. The anisotropy of this map was suggested by Lazarian et al. (2002) to be used to study the magnetic field direction. Later the anisotropies were studied us-

ing centroids in Esquivel & Lazarian (2005). Subsequently, the anisotropies were studied using the Principal Component Analysis (PCA) in Heyer et al. (2008), which is the way of studying anisotropies that equivalent to the aforementioned centroid technique.

The technique of using velocity centroid correlation function anisotropy (CFA) to probe the direction of magnetic fields was further elaborated in (Esquivel & Lazarian 2011) and was presented as a technique to study magnetization, i.e. the Alfvén Mach number M_A of turbulence. Potentially, one can apply the technique to smaller patches of sky to map the local direction of magnetic fields. However, applying of the correlations assumes that the averaging over an ensemble of realizations is available (see Monin & Jaglom 1975). In practical terms this means that the volume averaging is performed over the patch of the sky much larger than the correlation scale of the eddies. This contradicts the idea of *local* measurements and the corresponding weakness of this approach of detailed tracing magnetic fields is illustrated below.

The CFA technique relies on the statistics of correlation over a large patch of data to give a clear anisotropy. However, when the patches used for correlation are not large, the shape of the correlation function becomes uncertain, hence a prediction from such calculation fails to trace the local direction of magnetic fields. In other words, it is difficult to apply CFA for probing the detailed structure of magnetic fields. In fact, our study of Synchrotron Intensity Gradients (SIGs) in LYLC showed the *AM* of SIGs is significantly better than that of CFA on smaller scales, and becomes comparable only at the largest scales.

To perform the same test as in LYLC, we selected a cube and performed a *AM*-block test for velocity centroids and intensity maps. Guided by (Esquivel & Lazarian 2011) we developed an algorithm for calculating the CFA. As the correlations get elongated along the magnetic field direction, the maximum gradient is perpendicular to it. We therefore calculate the gradients within the correlation function space, and rotate 90 degrees to acquire the field direction prediction. To

compare the sub-block average vectors from our recipe, we use the same block to calculate the correlation function. This enables the CFA to have local predictions like the VCGs.

Figure 11 shows the comparison of AM for these two methods. While in principle the alignment from CFA is improving as the block size increases, VCG still shows a better alignment in large scales. In small scales, CFA does not show any preferential alignment. In contrast, the alignment of VCG remains positive over all scales. That indicates the superiority of using VCG over CFA in *all* scales.

6. CONCLUSION

Our paper confirms the advantages of the VCGs for probing the ISM processes. We confirmed that in the diffuse media the VCGs trace the magnetic field well and showed that they can also be efficient in identifying the regions dominated by self-gravity. The advantages of the VCGs include relatively low requirements on observation data, easiness of applications, and rich physics that can be unearthed as the result of the application of the technique. We demonstrate both the superiority of the VCGs over the IGs and CFA in terms of the magnetic field tracing, and stress the synergy of the techniques for the ISM studies. The results in the paper can be briefly summarized:

1. We tested how VCGs and IGs behave under different physical conditions, including a change of sonic and Alfvénic Mach numbers. We also tested the technique in slightly super-Alfvénic environment. From our tests we showed a systematic superiority of VCGs over IGs on tracing magnetic fields in diffuse media. We also showed that the deviations of the direction of the VCGs and the IGs can signify the existence of shocks.

2. We also demonstrated new ways to improve the performance of the VCG technique in terms of tracing magnetic fields by (1) Removing pixels with higher gradient amplitudes, and (2) Removing the contribution of lower wave number. This makes the VCG magnetic field tracing more reliable.
3. For self-gravitating regions we demonstrated that the alignment of the VCGs changes. In the case of dynamically important magnetic field, the unconstrained falling of matter along magnetic fields lines makes the gradients aligned with magnetic fields. Therefore the change of the relative orientation of polarization directions and those determined by the VCGs can provide the observational signature of the self-gravitating collapse within molecular clouds.
4. We compare the VCG magnetic field tracing to the tracing that employs the correlation function anisotropy technique. We demonstrate a significant advantage of tracing magnetic fields using the VCGs compared with magnetic field tracing based on correlation anisotropies.

The stay of KHY at UW-Madison is supported by the Fulbright-Lee Hysan research fellowship and Department of Physics, CUHK. AL acknowledges the support the NSF grant AST 1212096, NASA grant NNX14AJ53G as well as a distinguished visitor PVE/CAPES appointment at the Physics Graduate Program of the Federal University of Rio Grande do Norte, the INCT INEspao and Physics Graduate Program/UFRN.

REFERENCES

- Andersson, B.-G., Lazarian, A., & Vaillancourt, J. E. 2015, *ARA&A*, 53, 501
- Beresnyak, A., Lazarian, A., & Cho, J. 2005
- Brandenburg, A., & Lazarian, A. 2013, *Space Science Reviews*, Volume 178, Issue 2-4, pp. 163-200, 178, 163
- Brunt, C. M., & Heyer, M. H. 2002, *ApJ*, 566, 276
- Cho, J., & Lazarian, A. 2002, 4
- Cho, J., & Lazarian, A. 2003, *Monthly Notices of the Royal Astronomical Society*, 345, 325
- Cho, J., & Vishniac, E. T. 2000, *The Astrophysical Journal*, Volume 539, Issue 1, pp. 273-282., 539, 273
- Clark, S. E., Hill, J. C., Peek, J. E. G., Putman, M. E., & Babler, B. L. 2015, *Physical Review Letters*, 115, 1
- Draine, B. T. 2009, in *Astronomical Society of the Pacific Conference Series*, Vol. 414, *Cosmic Dust - Near and Far*, ed. T. Henning, E. Grün, & J. Steinacker, 453
- Draine, B. T. 2011, *Physics of the interstellar and intergalactic medium* (Princeton University Press), 540
- Esquivel, A., & Lazarian, A. 2005, *ApJ*, 631, 320
- . 2011, *ApJ*, 740, 117
- Esquivel, A., Lazarian, A., & Pogosyan, D. 2015, *ApJ*, 814, 77
- Gaensler, B. M., Haverkorn, M., Burkhart, B., et al. 2011, *Nature*, Volume 478, Issue 7368, pp. 214-217 (2011), 478, 214
- Goldreich, P., & Sridhar, S. 1995, *The Astronomical Journal*, 438, 763
- González-Casanova, D. F., & Lazarian, A. 2016
- Hayes, J. C., Norman, M. L., Fiedler, R. A., et al. 2006, 188
- Heyer, M., Gong, H., Ostriker, E., & Brunt, C. 2008, *ApJ*, 680, 420
- Kandel, D., Lazarian, A., & Pogosyan, D. 2016, *MNRAS*, 461, 1227
- . 2017, *MNRAS*, 464, 3617
- Kowal, G., & Lazarian, A. 2010, *Arxiv preprint*, 16
- Kowal, G., Lazarian, A., & Beresnyak, A. 2007, *ApJ*, 658, 423
- Kowal, G., Lazarian, A., Vishniac, E. T., & Otmianowska-Mazur, K. 2009, *ApJ*, 700, 63
- Lazarian, A. 2006, *ApJ*, 645, L25
- Lazarian, A. 2007, *JQSRT*, 106, 225
- Lazarian, A., Pogosyan, D., & Esquivel, A. 2002, in *Astronomical Society of the Pacific Conference Series*, Vol. 276, *Seeing Through the Dust: The Detection of HI and the Exploration of the ISM in Galaxies*, ed. A. R. Taylor, T. L. Landecker, & A. G. Willis, 182
- Lazarian, A., & Vishniac, E. T. 1999, *The Astrophysical Journal*, Volume 517, Issue 2, pp. 700-718., 517, 700
- Lazarian, A., Yuen, K. H., Lee, H., & Cho, J. 2017, *ArXiv e-prints*, [arXiv:1701.07883](https://arxiv.org/abs/1701.07883)
- Lithwick, Y., & Goldreich, P. 2001, *The Astrophysical Journal*, Volume 562, Issue 1, pp. 279-296., 562, 279
- Maron, J., & Goldreich, P. 2000, *The Astrophysical Journal*, Volume 554, Issue 2, pp. 1175-1196., 554, 1175
- Monin, A. S., & Iaglom, A. M. 1975, *Statistical fluid mechanics: Mechanics of turbulence*. Volume 2 /revised and enlarged edition/
- Norman, M. L. 2000, 6, 6

Soler, J. D., Hennebelle, P., Martin, P. G., et al. [2013](#), [16](#)

Tofflemire, B. M., Burkhart, B., & Lazarian, A. 2011, [ApJ](#), [736](#), [60](#)

Truelove, J. K., Klein, R. L., Mckee, C. F., et al. 1997

Yuen, K. H., & Lazarian, A. 2017, ArXiv e-prints, [arXiv:1701.07944](#)